Design and Evaluation of a Bowden-Cable-Based Remote Actuation System for Wearable Robotics

Journal Article

Author(s):
Hofmann, Urs A.T.; Butzer, Tobias; Lambercy, Olivier; Gassert, Roger

Design and Evaluation of a Bowden-Cable-Based Remote Actuation System for Wearable Robotics

Urs A. T. Hofmann, Tobias Bützer, Olivier Lambercy, and Roger Gassert

Abstract—Wearable robots can assist motor-impaired individuals in activities of daily living, but weight is paramount for usability. Proximally placed actuators and remote actuation systems (RAS) minimize weight on users' extremities. State-of-the-art RAS employ pneumatics, hydraulics, or Bowden cables, which all have considerable limitations. Here, we present a novel Bowden-cable-based bidirectional RAS featuring high power-to-mass and power-to-volume ratios, easily accessible components, and compact mechanical design. A rack-and-pinion mechanism reduces the force transmitted through the Bowden cables, permitting use of extremely compliant sheaths. The feed-forward friction compensation model, integrated bending angle sensor, and series elastic elements ensure accurate force control across all bending angles of the Bowden cables and the user's full range of motion. As a proof-of-concept a RAS was designed for a hand exoskeleton with a maximal output force of 150 N. With a power-to-volume and a power-to-mass ratio of 127 kW/m^3 and 56 W/kg at the output, and of 2.0 kW/m^3 and 1.6 W/kg for the entire system, it outperforms other state-of-the-art RAS. With the implemented speed- and current limiting, the system operates for at least 2 h continuously. It is water- and dustproof, meeting hygienic and practical demands. Importantly, this novel system can be scaled to the requirements of various applications in wearable robotics.

Index Terms—Force Control, Sensor-based Control, Wearable Robotics, Mechanical power transmission, Prosthetics and Exoskeletons

I. INTRODUCTION

WEARABLE assistive devices are a promising approach to enhance the remaining functional abilities of neurological patients (e.g. after a stroke or a spinal cord injury), and potentially provide further rehabilitation training. In the past decade alone, over 140 hand exoskeletons have been developed, 46 of which were declared as daily assistive devices [1]. In contrast to stationary rehabilitation devices [2], [3], wearable assistive tools are designed to be used and worn throughout the entire day and, therefore, are dramatically restricted in size and weight. In a study with 242 upper limb prosthesis users, low added weight to the arm was found to

All authors are with the Rehabilitation Engineering Laboratory, ETH Zurich, 8092 Zurich, Switzerland. *(Urs Hofmann and Tobias Bützer are co-first authors, e-mail:* `hofmannu@student.ethz.ch`, `tobias.buetzer@hest.ethz.ch`*).*

be the most important design factor [4] and in neurological patients added weight leads to faster fatigue. This underlines the difficult trade-off between a compact, wearable design and the mechanical complexity necessary to assist motor-impaired patients in activities of a daily living (ADL). While many devices feature clever mechanical solutions and various functions, many also introduce high perceived weight due to motors placed on extremities [5]–[8].

Remote actuation systems (RAS), such as presented in [9]–[12], typically consist of an actuation unit, a transmission system, and an output, where the force is applied to the environment. With RAS, motors can be moved to proximal body parts, which decreases the weight of the hand (where the output of the RAS is located), but also increases the overall weight of the system due to the additional mechanical structures needed for force transmission. Pneumatic RAS offer high power density at the output [13] and the compliance of the pressurized air can be beneficial for robotic systems interacting with humans. However, state-of-the-art air pressure generators are noisy and heavy. Furthermore, the trade-off for compliance is nonlinear control and a small achievable bandwidth [14]. Hydraulic RAS offer high power density at both the actuation unit and the output, and thanks to quasi-incompressible media, high bandwidths can be achieved [15]. However, hydraulic cylinders are affected by nonlinear friction, which makes control difficult and decreases efficiency [16]. More importantly, hydraulic lines stiffen with increasing pressure, limiting the range of motion (ROM) of the user. In addition, leakage can occur and lines can burst, potentially causing serious injuries. The most promising and most commonly used RAS in wearable robotics are systems based on Bowden cables [10], [11], [17]–[25]. The integration into existing systems driven by electromagnetic motors is straightforward, the needed components are easily accessible, and the cables operate safely. With properties such as low weight and volume, low noise emission, and compact mechanisms they address most of the limitations of other approaches. Drawbacks are backlash and nonlinear friction, which both depend on the overall bending angle of the transmission cables.

In our previous work, we presented and used a RAS for a hand exoskeleton, based on a bidirectional Bowden cable design [11]. It reduced the mass of the exoskeleton worn at the hand from 256 g to 113 g. However, stroke and spinal cord injury (SCI) patients revealed in a usability study that the stiffness of the Bowden cables leads to both high perceived weight and limited ROM of the arm.

In this paper we present the design and evaluation of a novel, portable RAS based on Bowden cable torque trans-

mission combined with a rack-and-pinion output mechanism. It benefits from the advantages of Bowden-cable-based RAS and accounts for their limitations: an integrated bending angle sensor allows to compensate for nonlinear friction, a reduction of the rope tension in the rack-and-pinion mechanism allows to use extremely compliant sheaths, and a feed-forward control approach based on the capstan equation accurately sets the output force directly from force measurements with series elastic elements (SEEs) at the actuation unit. Furthermore, water- and dustproof design and minimal power consumption increase the duration of operation. These are crucial factors for the application of the proposed RAS in wearable robotics. The developed actuation system can find application in various wearable robotic systems. In this paper, we present a RAS dimensioned and optimized for the specific case of a wearable hand exoskeleton intended for use during ADL in the home environment as a proof-of-concept. Furthermore, we directly compare the new system to the Bowden-cable-based solution previously presented by our group [11].

II. Design

A. Application-specific requirements

Ideally, a RAS transmits forces or torques with minimal loss from the actuation unit to the output. Requirements for RAS used in wearable robotics include high power densities of both the overall system and the output to ensure low mass, accurately controllable output force to safely interact with the user, and appealing design including appearance, ergonomics as well as low noise emission to achieve high user acceptance. For increased usability, unrestricted ROM of the user and a water- and dustproof transmission system and output are desired. Keeping size restrictions in mind, the motors should be powered off whenever possible such that a small battery can be used. Lastly, the system should be scalable to different force and speed requirements defined by different applications.

The hand exoskeleton used for the proof-of-concept application of the proposed RAS is based on the three-layered spring finger mechanism presented in [26]. The finger mechanism requires an accurately controlled input force of $30\,\mathrm{N}$ per finger. To provide dexterity but maintain a compact and lightweight mechanical design, we decided to couple the motion of all fingers except for the thumb as suggested in [27]. Consequently, the needed force adds up to a total of $120\,\mathrm{N}$ for the four coupled fingers. The mechanism requires a linear stroke of $25\,\mathrm{mm}$ for full flexion of the fingers. To perform ADL, hand opening and closing at $0.5\,\mathrm{Hz}$ is targeted, leading to an output speed of $25\,\mathrm{mm\,s^{-1}}$. The battery runtime should be at least $2\,\mathrm{h}$ for use in daily living. The transmission system will be guided along the human body from the actuation unit located at the user's back to the output located at the user's hand [11]. In order not to restrict shoulder or elbow motion, the transmission system should be very flexible and allow for bending angles up to $180°$ ($90°$ shoulder and $90°$ elbow).

B. System overview

The proposed RAS consists of an input winch at the actuation unit and an output winch at the output, as illustrated in Fig. 1. The winches are connected by two ropes, winded in opposite directions and guided through thin and highly compliant spiral stainless steel sheaths (Bowden cables). A stepper motor drives the input winch. At the output winch, a rack-and-pinion mechanism converts rotation to linear motion and torque to force. The output force is controlled via a feed-forward model based on the rope tension and the overall bending angle of the Bowden cables. Two SEEs in the actuation unit are used to pretension the ropes and to measure the rope tension. The overall bending angle of the Bowden cables is measured by a custom-built sensor based on a third, independent wire. Force and velocity outputs can be scaled by adapting winch diameters and rack-and-pinion gear ratio.

C. Mechanical analysis and dimensioning

The output force F_{out} at the rack relates to the input torque at the input winch τ_{in} according to:

$$F_{out} = \frac{\exp(-\mu \cdot \sigma) \cdot r_{w,o} \cdot \eta}{r_{w,i} \cdot r_{pi}} \cdot \tau_{in} \tag{1}$$

where μ coefficient of friction in Bowden cable
σ bending angle of Bowden cable
$r_{w,o}$ radius of output winch
r_{pi} pitch radius of pinion
$r_{w,i}$ radius of input winch
η efficiency of rack-and-pinion mechanism.

The transmission efficiency of the Bowden cables ($1.2\,\mathrm{m}$ wire traction drive technology, MELTIN MMI, Japan) is defined as the ratio between output and input rope tension $F_{t,o}/F_{t,i}$ and described by the capstan equation for a flexible line wound around a cylinder represented by the term $\exp(-\mu\cdot\sigma)$ in (1). The overall bending angle σ and the friction coefficient μ between rope and sheath consequently influence the transmission efficiency. Pretension, bending radius, rope velocity, and input force can be considered as having negligible effects [28], [29].

Transmitting high rope tension requires stiff sheaths to withstand high compression forces. To keep the transmission system lightweight and compliant while providing sufficient output force, we reduced the rope tension by optimizing the mechanical components according to (1) and setting the gear ratio of the receiving mechanism to five ($r_{w,r} = 12.5\,\mathrm{mm}$, $r_{pi} = 2.5\,\mathrm{mm}$). The input winch was designed with a small radius ($r_{w,s} = 3.6\,\mathrm{mm}$) for a high force-to-velocity ratio of the rope, favoring the optimal work point of the stepper motor.

The housing and winches were custom made. A gear with ten teeth and a modulus of 0.5 (10 Z M 0.5, Reely, Germany) and a $40\,\mathrm{mm}$ long rack (polyactal rack M 0.5, Reely, Germany) form the rack-and-pinion mechanism. At the output, two bearings (RC-Car ball bearing, $D_i = 3\,\mathrm{mm}$, $D_o = 7\,\mathrm{mm}$, Reely, Germany) guide the axis on which both gear and output winch are mounted. To reduce the load acting on the motor shaft, the input winch is guided by two radial bearings (RC-Car ball bearing, $D_i = 10\,\mathrm{mm}$, $D_o = 15\,\mathrm{mm}$, Reely, Germany).

D. Actuation and power supply

Equation 1 relates the application specific requirements to the needed motor characteristics: in our proof-of-concept
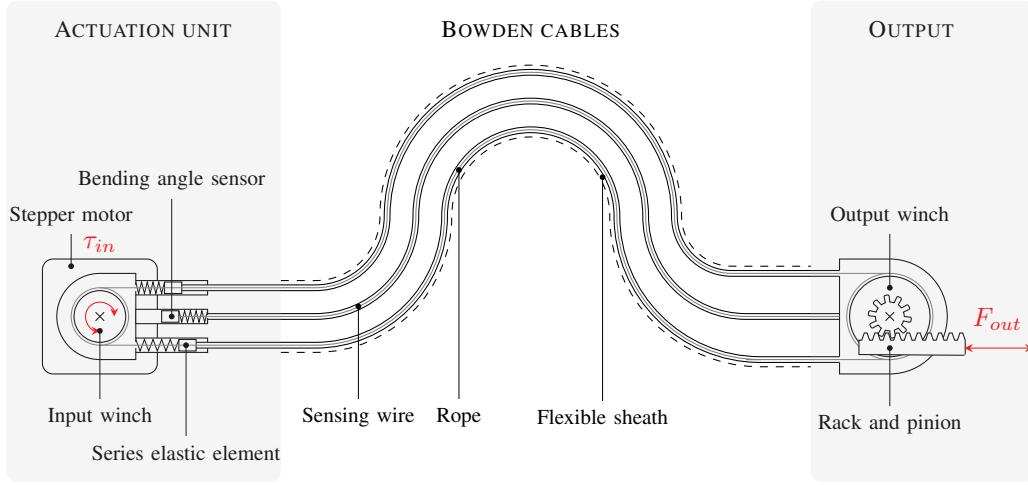
Fig. 1. Working principle of the Bowden-cable-based actuation system: ropes guided in flexible sheaths connect the input winch to the output winch. The input winch is driven by a stepper motor. At the output, a rack-and-pinion mechanism converts torque into force. The output force is controlled via a feed-forward model based on the rope tension and the overall bending angle of the Bowden cables. The integrated bending angle sensor is based on a sensing wire, guided along the Bowden cables.

application a torque of $0.2\,\mathrm{N\,m}$ has to be delivered at a speed of up to $270\,\mathrm{rpm}$ to the input winch. A stepper motor (NEMA 17, QSH4218-35-10-027, Trinamic, Germany) was chosen for high torque-to-velocity ratio.

A small size, low voltage stepper motor driver (DRV8834 Low-Voltage Stepper Motor Driver Carrier, Pololu, USA) drives the motor and is supplied with $10.4\,\mathrm{V}$, down-regulated from a $11.1\,\mathrm{V}$ lithium polymer battery (Sway-FPV LiPo 3S $11.1\,\mathrm{V}$ $1500\,\mathrm{mA\,h}$ 60C/120C XT60, Swaytronic, Switzerland). The driver was preset to half-stepping, which decreases the motor speed but increases the achievable torque. The motor driver includes a screw-type potentiometer to adjust the voltage setting the maximal coil current and protect the motor coils against overheating. The potentiometer was replaced with a resistor-capacitor (RC) element connected to a pulse width modulation (PWM) output of a microcontroller (Arduino DUE, Arduino AG, Italy). With this setup, the maximal coil current can be controlled electronically. A good trade-off between low load time of the capacitor τ and high equalization G was found at $C = 2.2\,\mathrm{\mu F}$ and $R = 12\,\mathrm{k\Omega}$, leading to $G = 2.65 \times 10^6$ and $\tau = 26.4\,\mathrm{ms}$ (Arduino DUE: $f_{PWM} = 16\,\mathrm{MHz}$).

E. Sensing and force control

A strong requirement was that electronics are placed only at the actuation unit, making both transmission system and output inherently resistant to spray water and dust exposure during ADL, reducing their mass and volume at the same time. To control the output force from forces measured at the actuation unit, a feed-forward model based on (1) is used. It relates the output force F_{out} to the input torque τ_{in}, depending on the overall bending angle σ and several constants. Therefore, τ_{in} and σ need to be measured continuously.

Two SEEs are used to determine the input torque τ_{in} (Fig. 2). They are composed of linear potentiometers (PTA 3043-2010 CP B 503, BOURNS, USA), which measure the

positions x_1 and x_2 of sliders connecting the sheaths to compression springs ($3.338\,\mathrm{N\,mm^{-1}}$, D-173J, Gutekunst + Co KG., Germany). The compression springs are used to pretension the cable and eliminate backlash, and to measure rope tension from the displacement of the slider. When tension is applied to the ropes, the sheaths are loaded with the reacting compression force. Each SEE measures the force acting on one sheath based on the deformation of the spring according to

$$F_{r,n} \approx F_{s,n} = k \cdot (L_0 - x_n), \ n \in \{1, 2\} \tag{2}$$

where
$F_{r,n}$	force acting on rope n
$F_{s,n}$	force acting on spring n
k	spring constant
L_0	zero length
x_n	length of spring n.

The input torque τ_{in} corresponds to:

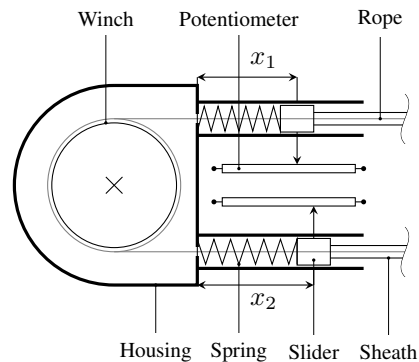$$\tau_{in} = (F_{r,2} - F_{r,1}) \cdot r_{w,s}. \tag{3}$$

Fig. 2. Rope tension measurement with series elastic elements: linear potentiometers measure the positions x_1 and x_2 of sliders attached to the sheaths on one side and to compression springs on the other side. Compression force acting on the sheaths, which develops in reaction to tension in the rope, can be measured through the deformation of the springs.

A bending angle sensor based on a principle presented in [30] is used to measure the bending angle σ in an additional wire (sensing wire). Sheath and rope are fixed relatively to each other at the output. Bending introduces differences in path lengths between rope and sheath, and therefore influences the position of the slider at the actuation unit. A small permanent magnet (MAGNET 4.2, MEDER, USA) is attached to the slider. A Hall effect sensor (Radiometric Sensor, linear, SS495 A, Honeywell, USA) measures the magnetic field changes depending on the distance between magnet and sensor (Fig. 3).
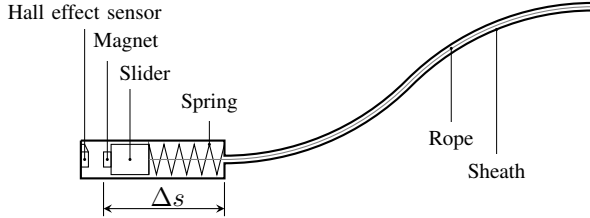

Fig. 3. Bending angle sensor: in a separate wire, independent of the Bowden cables, a spring-loaded rope is guided through a sheath. When rope and sheath bend, a difference in the path length induces a movement of a slider attached to the rope. A Hall effect sensor measures the displacement Δs of a permanent magnet attached to the slider. From Δs the overall bending angle σ can be estimated.

Using the SEEs, a closed-loop PID controller controls the speed of the motor towards a setpoint of τ_{in}, which is given by the feed-forward model, fed with the desired output force of the RAS and the current bending angle σ. A photograph of the developed RAS including actuation unit, Bowden cables, and output is shown in Fig. 4.

F. Current- and speed limiting

The required motor coil current changes as a function of the acting torque τ_m. To save energy, the coil current I_c is adapted dynamically using the PWM output and the RC element described in Sec. II-D. For the presented system, we determined the relation between required coil current I_c and motor torque τ_m experimentally: for various constant current levels I_c the motor torque τ_m was increased until motor stall. To safely control the RAS we use a fixed value of 1.8 A while the motor is moving, and linear relation (linear fit of the measured results) between I_c and τ_m, while the motor is in a static position:

$$I_c = \begin{cases} 2.4 \ \frac{A}{Nm} \cdot \tau_m & \text{if } I_c \leq 1.8 \text{ A} \\ 1.8 \text{ A} & \text{if } I_c > 1.8 \text{ A} \end{cases}. \quad (4)$$

When the motor runs at high velocities and high torques, misstepping can occur even at maximal coil current. Consequently, the system becomes unstable and difficult to control. To avoid misstepping while the motor is moving, we limit the speed of the motor to a dynamic maximum value ω_{max} depending on the acting torque τ_m (Fig. 5). The relation between maximum speeds ω_{max} for given torques τ_m was found experimentally: for various constant target forces the speed was increased until misstepping occurred. For the presented

system, we use a linear relation (linear fit of the measured results) between maximum achievable velocity of the motor ω_{max} and acting motor torque τ_m, which is expressed as rope tension F_r acting on the input winch:

$$\omega \leq \begin{cases} 135, & \text{if } F_r \geq 42 \text{ N} \\ 630 - 11.8 \ \frac{1}{N} \cdot F_r, & \text{if } F_r < 42 \text{ N} \end{cases} \text{[rpm]}. \quad (5)$$

The maximum velocity ω_{max} decreases linearly with increasing force until a constant minimal velocity is reached. This creates a safe operation window for the PID controller in which misstepping does not occur (light gray shaded area, Fig. 5).
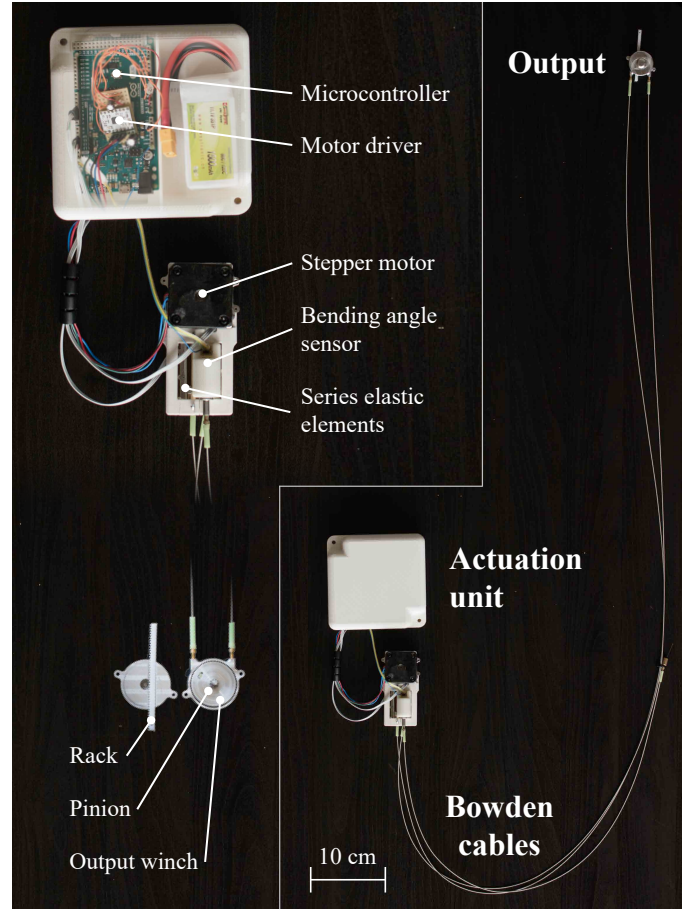

Fig. 4. Picture of the final prototype including actuation unit, Bowden cables, and output.

III. EVALUATION

A. Transmission efficiency of Bowden cables

To determine the coefficient of friction between the sheath and the rope μ, we measured the output rope tension $F_{t,o}$ as a function of different input tensions $F_{t,i}$ (0 N to 70 N in steps of 5 N) and bending angles σ (0° to 180° in steps of 30°) with a force gauge (Advanced Force Gauge 100 N, Mecmesin, UK). The results are shown in Fig. 6.

The capstan equation

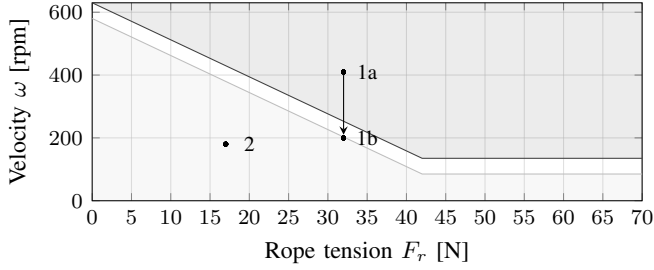$$F_{t,o} = F_{t,i} \cdot \exp(-\mu \cdot \sigma) \quad (6)$$

Fig. 5. Dynamic speed limiting: within the dark gray area, misstepping of the stepper motor can occur due to too high velocity. Therefore, the motor speed set by the PID controller is limited to a maximum value depending on the acting force (light gray line) and working points outside of this area (1a) are shifted to the light gray shaded window of safe operation for the currently acting force (1b). Within the window of safe operation misstepping does not occur. For those working points (2) the output of the PID controller is used without further processing.
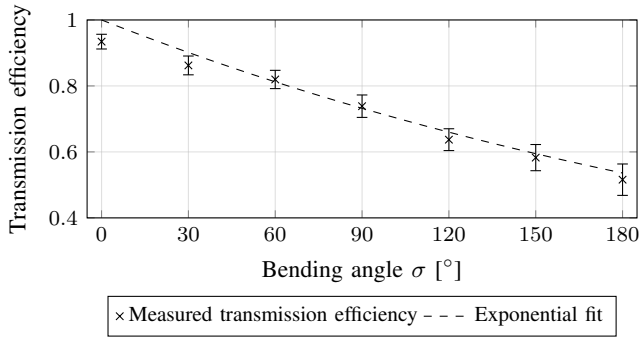

Fig. 6. Force transmission efficiency as a function of bending angle σ: the efficiency decreases exponentially with increasing bending angle, following the capstan equation. A coefficient of friction $\mu = 0.20$ resulted in the best fit. In the proof-of-concept application with a hand exoskeleton bending angles from $90°$ to $180°$ can be expected.

was fitted to a calibration dataset, indicating that μ is approximately 0.20 (dashed line, Fig. 6).

B. Bending angle estimation

The accuracy of the bending angle sensor was evaluated by measuring the total bending angle of the Bowden cables with a calibrated rotary potentiometer (Precision Potentiometer Model 533, Vishay Spectrol, USA), and the Bowden-cable-based sensor at the same time (Fig. 7).

The Bowden-cable-based sensor measures the bending angle with a mean absolute error (MAE) of $5.50°$ and a mean absolute percentage error (MAPE) of 9.7%.

C. Maximal output force and power

The power output of the system P (mechanical work per time $\Delta W / \Delta t$) was measured with a tension spring (2.5 x De 17.5 x 126.0, n 40, k = $3.023\,\mathrm{N\,mm^{-1}}$, Durovis, Luxembourg), which connected a force gauge (LSB 302, FUTEK, USA) to the rack of the output. The properties of the spring were chosen such that it emulated the mechanical properties of the hand
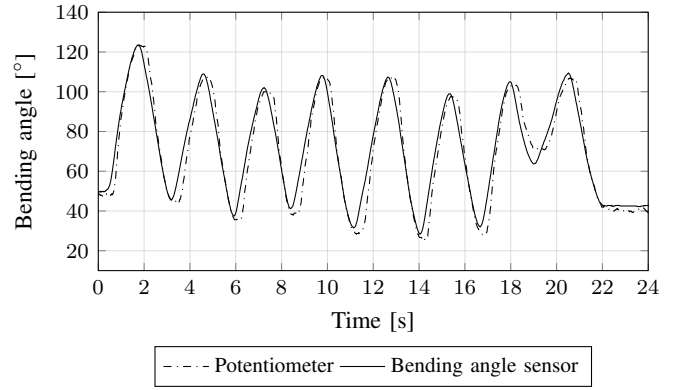

Fig. 7. Accuracy of the bending angle measurement: the bending angle was measured simultaneously with a calibrated potentiometer (dashed line) and the developed sensor (solid line).

exoskeleton. In this setup, the RAS was used to tension the spring from a force F_1 to $F_2 > F_1$:

$$P = \frac{k \cdot (F_2{}^2 - F_1{}^2)}{2 \cdot \Delta t}. \tag{7}$$

The resulting maximal output power was $(1.11 \pm 0.04)\,\mathrm{W}$.

We tested the maximal output force of the system at a bending angle of $0°$. The output force was increased stepwise until motor stall. The maximal force at the rack was $(150 \pm 5)\,\mathrm{N}$ in both directions.

D. Force control accuracy

We evaluated the accuracy of the feed-forward force controller at a bending angle of $0°$ using step, ramp, and sinus functions as input signals (solid lines, Fig. 8). For each signal, the output target force of the controller was continuously updated. The actual force at the rack (dashed lines, Fig. 8) was measured with a force gauge (LSB 302, FUTEK, USA).

The MAE between target and actual force was $1.6\,\mathrm{N}$ (MAPE 6.6%) for the step response. The controller reached the setpoint after less than $0.5\,\mathrm{s}$. Returning to the initial setpoint took approximately $1.8\,\mathrm{s}$. The controller followed the ramp with a MAE of $0.8\,\mathrm{N}$ (MAPE 1.9%). For the sinus function ($0.5\,\mathrm{Hz}$), a phase shift between target and actual force was observed. This leads to a much higher MAE of $7.1\,\mathrm{N}$ (MAPE 19.4%).

The accuracy of the feed-forward friction compensation at varying bending angles of the Bowden cables was tested from $0°$ to $150°$ in steps of $30°$. The ramp function matches the load patterns of the exoskeleton best and was tested at each angle both without and with friction compensation. When the bending angle sensor was disabled and the feed-forward friction compensation only compensated for typical friction losses at a bending angle of $0°$, the MAE increased with increasing bending angle of the Bowden cables. When the bending angle sensor was enabled and the feed-forward friction compensation was updated accordingly, forces were controlled with a MAE constantly below $2\,\mathrm{N}$ (MAPE below 5%).

(a) Step response

(b) Ramp response

Time [s]

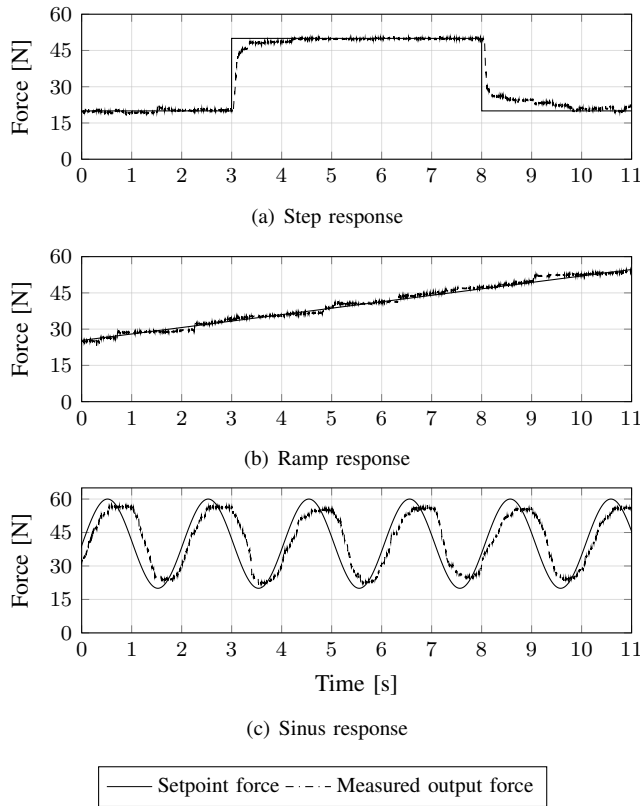(c) Sinus response

—— Setpoint force – · – · Measured output force

Fig. 8. Accuracy of the proposed feed-forward controller at a constant bending angle of 0°: From top to bottom, step, ramp, and sinus functions were fed to the controller as setpoint forces (dashed line) and are shown together with the corresponding output force of the RAS (solid line). The output force was measured at the rack with a calibrated force gauge.

Bending angle [°]
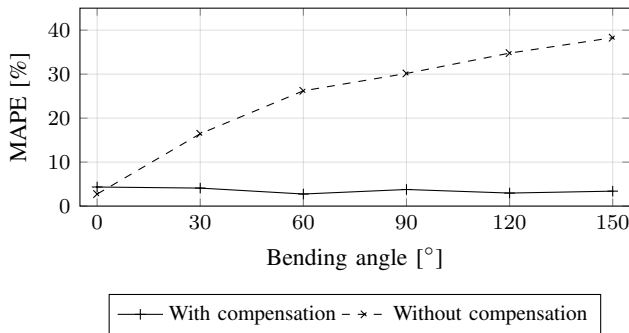
—+— With compensation – ✳ – Without compensation

Fig. 9. Mean absolute percentage error (MAPE) of the output force control both with enabled and disabled feed-forward friction compensation at different bending angles. While the MAPE increases with increasing bending angle without compensation (dashed line), it stays below 2 N with enabled compensation (solid line).

E. Power-to-mass and power-to-volume ratio

We evaluated weight and volume of each part of the RAS, including actuation unit, transmission system, and output. For an objective comparison to other systems, relative values were used, as recommended in [31]. Power-to-mass ratio P_m and power-to-volume ratio P_v are thereby defined as:

$$P_m = P/m; \; P_v = P/V \qquad (8)$$

where
P mechanical output power of the entire system
m mass of a component or the entire system
V volume of a component or the entire system.

With the measured mechanical power (Sec. III-C), we calculated the P_m and P_v of each part (Tab. I). For comparison, we also provide the values of the RAS previously developed by our group, in which push-pull Bowden cables were used [11].

TABLE I
PROPERTIES OF THE NEW AND PREVIOUS RAS.

	New RAS	Previous RAS [11]
Maximum output force [N]		
Pushing	150 ± 5	28 ± 4
Pulling	150 ± 5	28 ± 4
Mass [g]		
Actuation unit	516 ± 10	127 ± 6
Transmission system	33 ± 1	31 ± 1
Output	20 ± 1	5 ± 0
Overall	569 ± 10	163 ± 6
Volume [cm³]		
Actuation unit	682 ± 8	77 ± 4
Transmission system	6 ± 1	6 ± 1
Output	9 ± 0	2 ± 0
Overall	697 ± 8	85 ± 4
Power-to-mass ratio [W/kg]		
Actuation unit	2.2 ± 0.1	1.2 ± 0.3
Transmission system	34 ± 2	5 ± 1
Output	56 ± 3	30 ± 8
Overall	2.0 ± 0.1	0.9 ± 0.3
Power-to-volume ratio [kW/m³]		
Actuation unit	1.6 ± 0.1	6.0 ± 1.4
Transmission system	184 ± 24	24 ± 7
Output	127 ± 5	85 ± 23
Overall	1.6 ± 0.1	1.8 ± 0.5

IV. DISCUSSION AND CONCLUSION

We presented a novel RAS, which combines Bowden-cable-based bidirectional torque transmission with a rack-and-pinion mechanism, an integrated bending angle sensor, and a feed-forward friction compensation model in order to improve the power-to-mass and power-to-volume ratios as well as the controllability compared to other RAS. Current limitations of Bowden-cable-based transmission systems such as nonlinear friction, backlash, and stiff transmission wires are addressed, while the overall RAS and the output are extremely lightweight. As a proof-of-concept we evaluated a version of the proposed RAS dimensioned and optimized for the specific case of a wearable hand exoskeleton.

The proposed feed-forward compensation model calculates friction losses in the Bowden cable based on the capstan equation and inputs from an integrated bending angle sensor, guided in a separate Bowden cable. Two SEEs located in the actuation unit eliminate backlash by pretensioning the rope and allow for accurate bidirectional force control at varying angles of the Bowden cables by continuously measuring the spring

deformation and, therefore, rope tension. In contrast to related work [10], [11], [19], [23], all electronics are placed in the actuation unit, making both transmission system and output inherently water- and dustproof, which is crucial for use in real-world ADL assistance scenarios. The selected rack-and-pinion mechanism at the output reduces rope tension to 20% of the output force. This reduction of transmitted force through the Bowden cables allows to use very compliant and thin Bowden cables, which provide full and unperturbed arm ROM when wearing the device. Speed limiting avoids misstepping of the stepper motor, while coil current limiting saves up to 40% of energy, depending on the operation mode.

Compared to the RAS previously developed by our group [11], we doubled the power-to-mass ratio of both the entire system and the output. Power-to-mass and power-to-volume ratios of the transmission system were increased by a factor of six, while keeping the overall power-to-volume ratio in a similar range. A large number of Bowden-cable-based RAS intended for the use with wearable robots have been presented and summarized in reviews such as [1], [18]. Most state-of-the-art systems for which the maximum output force is reported cannot provide forces higher than $50\,\mathrm{N}$ [11], [24], [29], [32]. In [33] a Bowden-cable-based RAS for the use in a soft robotic exosuit for walking assistance was presented and output forces of up to $234\,\mathrm{N}$ were reported. However, with a total weight of $10.1\,\mathrm{kg}$, that system is significantly heavier than the system presented here. Pneumatic artificial muscles (PAMs) are known for their high power density, and are a common solution in wearable robotics [34], [35]. Nevertheless, the developed RAS is both more lightweight and smaller than a PAM-based solution with similar mechanical characteristics. An alternative hydraulic-based approach to transmit high mechanical power was presented in [15] and similar mechanisms are used in exoskeletons [36] and prostheses [37]. While the cylinders presented in [15] have similar mechanical performance, they are significantly heavier and bulkier than the developed RAS. With a MAPE below 5% independent of the bending angle, the accuracy of the force control is comparable to state-of-the-art actuation systems used in wearable robotics [36], [38]. Beside the winches, housings and two parts of the SEEs, all components used for the proof-of-concept prototype of the RAS are commercially available for a total cost of approximately $170\,\text{€}$.

The presented RAS was designed and tested for bending angles up to $180°$, forces up to $150\,\mathrm{N}$, and speeds up to $40\,\mathrm{mm\,s^{-1}}$ in the context of a proof-of-concept application to actuate a hand exoskeleton. However, the proposed concept can easily be scaled to different mechanical requirements by adapting the size of winches and gears. Furthermore, the concept holds a very broad range of output forces, speeds, and strokes. Therefore, the system can potentially be used to support further proximal body regions such as the lower extremity. It could eventually be adapted to fit the needs of various other applications where mass and volume are major design factors beyond the field of wearable robotics. To achieve forces higher than $150\,\mathrm{N}$, a more stable rack and bearings have to be selected. For mechanical output powers higher than $3\,\mathrm{W}$, the motor needs to be replaced by a more powerful alternative. By using a different Hall effect sensor, the measurable bending angle range can be increased [30].

As the SEEs measure the force acting on the sheaths, the force control is prone to external axial loads acting on the sheaths (e.g. accidental manual pulling on the Bowden cables). To prevent this, the wires have to be protected from external interaction, for example by a sleeve. The accuracy of the bending angle sensor could further be improved by reducing the friction acting on the slider or decreasing the difference between the inner diameter of the sheath and the outer diameter of the wire. The accuracy of the SEEs could be increased by using less stiff springs or more accurate potentiometers.

The presented RAS has been integrated into a hand exoskeleton and successfully tested in a preliminary usability test approved by the cantonal ethics commission of Zurich (Approval No. Req-2016-00656). The two subjects with severe upper limb impairment (one male, upper extremity Fugl-Meyer (FM) [39] score 45, and one female, upper extremity FM score 17, both subjects over 1 year post stroke) stated that the perceived weight from the RAS was highly acceptable and the flexibility of the transmission system has largely been improved in comparison the the RAS presented in [11], leading to quasi-unrestricted arm ROM. Detailed usability studies will need to be performed to verify these subjective comments and further evaluate the concepts, mechanical improvements, as well as the potential to apply this technology in ADL.

REFERENCES

[1] R. A. Bos, C. J. Haarman, T. Stortelder, K. Nizamis, J. L. Herder, A. H. A. Stienen, and D. H. Plettenburg, "A structured overview of trends and technologies used in dynamic hand orthoses," *J. NeuroEng. Rehabil.*, vol. 13, pp. 1–25, 2016.

[2] A. Borboni, M. Mor, and R. Faglia, "Gloreha - hand robotic rehabilitation: Design, mechanical model, and experiments," *J. Dyn. Sys., Meas., Control.*, vol. 138, no. 11, Oct. 2016.

[3] F. Orihuela-Espina, G. F. Roldán, I. Sánchez-Villavicencio, L. Palafox, R. Leder, L. E. Sucar, and J. Hernández-Franco, "Robot training for hand motor recovery in subacute stroke patients: A randomized controlled trial," *J. Hand Ther.*, vol. 29, no. 1, pp. 51–57, Nov. 2016.

[4] E. Biddiss, D. Beaton, and T. Chau, "Consumer design priorities for upper limb prosthetics," *Disabil. Rehabil.*, vol. 2, no. 6, pp. 346–357, 2007.

[5] L. Cui, A. Phan, and G. Allison, "Design and fabrication of a three dimensional printable non-assembly articulated hand exoskeleton for rehabilitation," in *Conf Proc IEEE Eng Med Biol Soc*, August 2015, pp. 4627–4630.

[6] J. Iqbal, N. G. Tsagarakis, and D. G. Caldwell, "Design of a wearable direct-driven optimized hand exoskeleton device," in *4th Int Conf on Advances in Computer-Human Interactions*, Gosier, Guadeloupe, France, February 2011, pp. 142–146.

[7] B. W. Gasser and M. Goldfarb, "Design and performance characterization of a hand orthosis prototype to aid activities of daily living in a post-stroke population," in *Conf Proc IEEE Eng Med Biol Soc*, August 2015, pp. 3877–3880.

[8] M. A. Zhou and B.-T. Pinhas, "Rml glove - an exoskeleton glove mechanism with haptics feedback," *IEEE/ASME Trans Mechatron*, vol. 20, no. 2, pp. 641–652, Apr. 2015.

[9] V. Agrawal, E. J. Peine, and B. Yao, "Modeling of transmission characteristics across a cable-conduit system," *IEEE Trans Rob*, vol. 26, no. 5, pp. 914–924, Oct. 2010.

[10] A. Chiri, N. Vitiello, F. Giovacchini, S. Roccella, F. Vecchi, and M. C. Carrozza, "Mechatronic design and characterization of the index finger module of a hand exoskeleton for post-stroke rehabilitation," *IEEE/ASME Trans. Mechatron.*, vol. 17, no. 5, pp. 884–894, 2012.

[11] C. J. Nycz, T. Bützer, O. Lambercy, J. Arata, G. S. Fischer, and R. Gassert, "Design and characterization of a lightweight and fully portable remote actuation system for use with a hand exoskeleton," *IEEE Robot. Autom. Lett.*, vol. 1, no. 2, pp. 976–983, July 2016.

[12] A. Wege and G. Hommel, "Development and control of a hand exoskeleton for rehabilitation of hand injuries," in *2005 IEEE/RSJ Int Conf on Intelligent Robots and Systems*, Aug. 2005, pp. 3046–3051.

[13] G. Belforte, L. Gastaldi, and M. Sorli, "Pneumatic active gait orthosis," *Mechatronics*, vol. 11, pp. 301–323, 2001.

[14] R. Morales, F. J. Badesa, N. Garcia-Aracil, J. M. Sabater, and C. Perez-Vidal, "Pneumatic robotic systems for upper limb rehabilitation," *Med Biol Eng Comput*, vol. 49, pp. 1145–1156, 2011.

[15] J. P. Whitney, M. F. Glisson, E. L. Brockmeyer, and J. K. Hodgins, "A low-friction passive fluid transmission and fluid-tendon soft actuator," in *2014 IEEE/RSJ Int Conf on Intelligent Robots and Systems (IROS)*, Chicago, USA, September 2014, pp. 2801 – 2808.

[16] X. B. Tran, N. Hafizah, and H. Yanada, "Modeling of dynamic friction behaviors of hydraulic cylinders," *Mechatronics*, vol. 22, pp. 65 – 75, 2012.

[17] R. A. R. C. Gopura, K. Kiguchi, and D. S. V. Bandara, "A brief review on upper extremity robotic exoskeleton systems," in *6th International Conference on Industrial and Information Systems*, Sri Lanka, August 2011, pp. 346–351.

[18] R. A. R. C. Gopura, D. S. V. Bandara, K. Kiguchi, and G. K. I. Mann, "Developments in hardware systems of active upper-limb exoskeleton robots: A review," *Rob. Auton. Syst.*, vol. 75, pp. 203–220, 2016.

[19] P. Agarwal, J. Fox, Y. Yun, M. K. O'Malley, and A. D. Deshpande, "An index finger exoskeleton with series elastic actuation for rehabilitation: Design, control and performance characterization," *The International Journal of Robotics Research*, vol. 34, no. 14, pp. 1747–1772, 2015.

[20] M. Cempini, S. M. M. D. Rossi, T. Lenzi, M. Cortese, F. Giovacchini, N. Vitiello, and M. C. Carrozza, "Kinematics and design of a portable and wearable exoskeleton for hand rehabilitation," in *IEEE Int. Conf. on Rehabilitation Robotics*, Seattle, Washington USA, June 2013.

[21] M. Cempini, F. Giovacchini, N. Vitiello, M. Cortese, M. Moisé, F. Posteraro, and M. C. Carrozza, "Neuroexos: a powered elbow orthosis for post-stroke early neurorehabilitation," in *IEEE Engineering in Medicine and Biology Conference*, Osaka, July 2013, pp. 1–4.

[22] M. Cempini, M. Cortese, and N. Vitiello, "A powered finger–thumb wearable hand exoskeleton with self-aligning joint axes," *IEEE/ASME Trans. Mechatron.*, vol. 20, no. 2, pp. 705–716, April 2015.

[23] B. K. Dinh, L. Cappello, M. Xiloyannis, and L. Masia, "Position control using adaptive backlash compensation for bowden cable transmission in soft wearable exoskeleton," in *IEEE/RSJ Int. Conf. on Intelligent Robots and Systems (IROS)*, Daejeon, Korea, October 2016, pp. 5670–5676.

[24] H. In, B. B. Kang, M. Sin, and K.-J. Cho, "Exo-glove - a wearable robot for the hand with a soft tendon routing system," *IEEE Rob Autom Mag.*, vol. 22, no. 1, pp. 97–105, March 2015.

[25] C. J. Nycz, M. A. Delph, and G. S. Fischer, "Modeling and design of a tendon actuated soft robotic exoskeleton for hemiparetic upper limb rehabilitation," in *Conf. Proc. IEEE Eng. Med. Biol. Soc.*, Milan, Italy, August 2015, pp. 3889–3892.

[26] J. Arata, K. Ohmoto, R. Gassert, O. Lambercy, H. Fujimoto, and I. Wada, "A new hand exoskeleton device for rehabilitation using a three-layered sliding spring mechanism," in *IEEE Int Conf on Robotics and Automation (ICRA)*, Karlsruhe, Germany, May 2013, pp. 3902–3907.

[27] F. Montagnani, M. Controzzi, and C. Cipriani, "Independent long fingers are not essential for a grasping hand," *Sci Rep*, vol. 6, no. 35545, pp. 1–9, 2016.

[28] D. Chen, Y. Yun, and A. D. Deshpande, "Experimental characterization of bowden cable friction," in *2014 IEEE Int Conf on Robotics and Automation*, Hong Kong, China, May - June 2014, pp. 5927–5933.

[29] L. Chen, X. Wang, and W. L. Xu, "Inverse transmission model and compensation control of a single-tendon-sheath actuator," *IEEE Trans Ind Electron*, vol. 61, no. 4, pp. 1424–1433, March 2014.

[30] U. Jeong and K.-J. Cho, "A novel low-cost, large curvature bend sensor based on a bowden cable," *Sensors*, vol. 16, no. 961, pp. 1–20, 2016.

[31] J. C. Moreno, L. Bueno, and J. L. Pons, *Wearable Robots: Biomechatronic Exoskeletons*. John Wiley & Sons, 2008, ch. Wearable robot technologies, pp. 165–200.

[32] U. Jeong and K.-J. Cho, "A feasibility study on tension control of bowden-cable based on a dual-wire scheme," in *2017 IEEE International Conference on Robotics and Automation (ICRA)*, Singapore, May 2017, pp. 3690–3695.

[33] A. T. Asbeck, S. M. D. Rossi, K. G. Holt, and C. J. Walsh, "A biologically inspired soft exosuit for walking assistance," *Int. J. Rob. Res.*, vol. 34, no. 6, pp. 744–762, 2015.

[34] A. P. Tjahyono, K. C. Aw, H. Devaraj, W. Surendra, and E. Haemmerle, "A five-fingered hand exoskeleton driven by pneumatic artificial muscles with novel polypyrrole sensors," *Industrial Robot*, vol. 40, no. 3, pp. 251–260, 2013.

[35] J.-F. Zhang, C.-J. Yang, Y. Chen, Y. Zhang, and Y.-M. Dong, "Modeling and control of a curved pneumatic muscle actuator for wearable elbow exoskeleton," *Mechatronics*, vol. 18, no. 8, pp. 448–457, 2008.

[36] F. Bechet and K. Ohnishi, "Electro-hydraulic force transmission for rehabilitation exoskeleton robot," in *13th Int Workshop on Advanced Motion Control*, vol. 13, March 2014, pp. 260–265.

[37] G. Smit, D. Plettenburg, and F. C. van der Helm, "The lightweight delft cylinder hand, the first multi-articulating hand that meets the basic user requirements," *IEEE Trans Neural Syst Rehabil Eng*, vol. 23, no. 3, pp. 431–440, May 2014.

[38] I. Jo and J. Bae, "A force-controllable compact actuator module for a wearable hand exoskeleton," in *Proc of the 19th World Congr of the Int Federation of Automatic Control*, Cape Town, South Africa, August 2014, pp. 4453–4458.

[39] A. R. Fugl-Meyer, L. Jääskö, I. Leyman, S. Olsson, and S. Steglind, "The post-stroke hemiplegic patient," *Scand. J. Rehab. Med.*, vol. 7, pp. 13–31, 1975.